Neurobiology of Aging 84 (2019) 178–188

Contents lists available at ScienceDirect

Neurobiology of Aging

journal homepage: www.elsevier.com/locate/neuaging

Hippocampal pathology in amyotrophic lateral sclerosis: selective vulnerability of subfields and their associated projections

Foteini Christidi [a,1], Efstratios Karavasilis [b,1], Michail Rentzos [a], Georgios Velonakis [b], Vasiliki Zouvelou [a], Sofia Xirou [a], Georgios Argyropoulos [b], Ioannis Papatriantafyllou [c], Varvara Pantolewn [b], Panagiotis Ferentinos [d], Nikolaos Kelekis [b], Ioannis Seimenis [e], Ioannis Evdokimidis [a,2], Peter Bede [f,g,h,2,*]

[a] Department of Neurology, Aeginition Hospital, National and Kapodistrian University of Athens, Greece
[b] Department of Radiology, General University Hospital "Attikon", National and Kapodistrian University of Athens, Greece
[c] Age Day Care Center IASIS, Glyfada, Greece
[d] Department of Psychiatry, General University Hospital "Attikon", National and Kapodistrian University of Athens, Greece
[e] Department of Medical Physics, Medical School, Democritus University of Thrace, Alexandroupolis, Greece
[f] Department of Neurology, Pitié-Salpêtrière University Hospital, Paris, France
[g] Biomedical Imaging Laboratory, Sorbonne University, INSERM, Paris, France
[h] Computational Neuroimaging Group, Trinity Biomedical Sciences Institute, Trinity College Dublin, Ireland

ARTICLE INFO

Article history:
Received 19 April 2019
Received in revised form 10 July 2019
Accepted 10 July 2019
Available online 23 September 2019

Keywords:
Amyotrophic lateral sclerosis
Alzheimer's disease
Hippocampus
Memory
Motor neuron disease
Multimodal MRI
Diffusion tensor imaging
Tractography

ABSTRACT

Although hippocampal involvement in amyotrophic lateral sclerosis (ALS) has been consistently highlighted by postmortem studies, memory impairment remains under-recognized and the involvement of specific hippocampal subfields and their connectivity patterns are poorly characterized in vivo. A prospective multimodal neuroimaging study has been undertaken with 50 well-characterized ALS patients, 18 patients with Alzheimer's disease, and 40 healthy controls to evaluate their mesial temporal lobe profile. Patients with ALS and Alzheimer's disease have divergent hippocampal signatures. The cornu ammonis 2/3 subfield and the hippocampus-amygdala transition area are the most affected regions in ALS in contrast to Alzheimer's disease, where the presubiculum and subiculum are the most vulnerable regions. Tractography reveals considerable fornix and perforant pathway pathology in both patient groups. Mesial temporal lobe structures in ALS have a selective and disease-specific vulnerability profiles, and their white matter projections exhibit concomitant degeneration. Our combined gray and white matter analyses indicate a connectivity-based, network-defined involvement of interconnected temporal lobe structures as opposed to contiguous involvement of adjacent structures. Our findings underline the importance of screening for memory deficits and personalized management strategies in ALS.

1. Introduction

ALS is now universally recognized as a multisystem condition affecting frontotemporal, subcortical, and cerebellar regions beyond its hallmark motor cortex and spinal cord pathology. In contrast to the extensive literature of frontal and temporal changes in ALS, hippocampal involvement and memory deficits remain relatively under-recognized, despite pioneering longitudinal neuropsychology and neuroimaging studies (Christidi et al., 2018b).

Early neuropsychology studies in ALS have overwhelmingly focused on executive dysfunction (Abrahams et al., 1995a,b), which were subsequently complemented by the characterization of behavioral, visuospatial, and language deficits (Burke et al., 2016; Christidi et al., 2018a; Finegan et al., 2019b; Montuschi et al., 2015; Phukan et al., 2012; Pinto-Grau et al., 2018). Memory deficits have only recently been recognized in ALS (Beeldman et al., 2016; Christidi et al., 2018b) and are thought to impact on compliance with assistive devices, participation in clinical trials,

Conflict of interest: None.
Statement: the data contained in the manuscript being submitted have not been previously published, have not been submitted elsewhere and will not be submitted elsewhere while under consideration at Neurobiology of Aging.

* Corresponding author at: Computational Neuroimaging Group, Trinity College Dublin, 152-160 Pearse Street, Dublin 2, Ireland. Tel.: +353 1 896 1000; fax: +353 1 454 2043.
E-mail address: bedep@tcd.ie (P. Bede).
[1] Shared first-authorship.
[2] Shared senior-authorship.

0197-4580/$ – see front matter © 2019 Elsevier Inc. All rights reserved.
https://doi.org/10.1016/j.neurobiolaging.2019.07.019

adherence to therapy, and activities of daily living (Burke et al., 2017a; Caga et al., 2019).

Pharmacological studies of ALS continue to rely on survival and clinical scores as key outcome measures overlooking the biomarker potential of quantitative neuroimaging measures (Bede et al., 2018b; Chipika et al., 2019; Schuster et al., 2016). Furthermore, clinical trials in ALS overwhelmingly focus on motor disability and respiratory function and do not take extra-motor manifestations of the disease into account. Extra-motor involvement is an important contributor to clinical heterogeneity in ALS (Burke et al., 2017b; Feron et al., 2018; Omer et al., 2017), which is recognized as a key barrier to successful clinical trials (Mitsumoto et al., 2014).

Despite the co-occurrence of ALS and Alzheimer's disease (AD) (Frecker et al., 1990; Segers et al., 2012) and similar memory profiles (Machts et al., 2014), it is unclear if ALS is associated with a characteristic hippocampal signature distinct from AD. Although the majority of hippocampal studies in ALS focus on gray matter pathology (Bede et al., 2013b; Westeneng et al., 2015), hippocampal subfields and their respective white matter projections are ideally studied together to test emerging concepts of trans-synaptic spread and connectivity-based disease propagation.

Accordingly, we sought to characterize the hippocampal profile of ALS in contrast to healthy controls (HCs) and disease controls using multimodal neuroimaging and test the hypothesis that ALS is associated with a unique hippocampal signature.

2. Methods

2.1. Ethics approval

This prospective neuroimaging study has been approved by the institutional review board of the Aeginition University Hospital, and all participants provided informed consent before inclusion.

2.2. Participants

Fifty ALS patients with a diagnosis of "definite" or "probable" ALS based on the revised El Escorial criteria (Ludolph et al., 2015) have been included. A group of 18 unselected AD patients were included as disease controls, and 40 HCs were also included. The National Institute on Aging and Alzheimer's Association (NIA-AA) criteria were used to establish the diagnosis of AD (McKhann et al., 2011). All AD patients were "probable AD" by the current categorization guidelines. AD mimics have been reassuringly out ruled by standardized assessments for structural, vascular, and inflammatory brain changes (magnetic resonance imaging [MRI]); endocrine, infectious, and hematological profiling; and screening for depression by the Geriatric Depression Scale (Yesavage et al., 1982). The majority of patients with AD (n = 11) had cerebrospinal fluid (CSF) analyses for beta-amyloid and tau, and their CSF profile was consistent with the diagnosis of AD. Exclusion criteria for study participation included comorbid neurological conditions, established psychiatric illness, psychoactive medications that may affect memory performance, and a clinical diagnosis of frontotemporal dementia. Demographic and representative clinical data are shown in Table 1.

2.3. Memory assessment

Memory performance was evaluated using the Rey Auditory Verbal Learning Test; Babcock Story Recall Test, and the Rey-Osterrieth Complex Figure Test in the ALS group (Table 2), as part of a larger cognitive battery assessing other cognitive domains (Christidi et al., 2012). To exclude the confounding effect of depression or low mood, the ALS Depression Inventory (Ferentinos et al., 2011; Hammer et al., 2008) was also administered.

2.4. MRI data acquisition

All participants underwent standardized brain imaging on a 3 Tesla Philips Achieva-Tx MR scanner. A 3D T1-weighted sequence was acquired with a time of repetition (TR): 9.9 ms, echo time (TE): 3.7 ms, flip angle: 7°, voxel-size 1 × 1 × 1 mm, matrix size 244 × 240, 170 slices. DTI data were acquired with an axial single-shot spin-echo echo-planar imaging sequence with 30 diffusion encoding directions and the following parameters: TR: 7299 ms, TE: 68 ms, flip angle: 90°, field of view: 256 × 256 mm, voxel size: 2 × 2 × 2 mm, 70 slices. FLAIR data were acquired with TR 11000 ms, TI 2800 ms, TE 125 ms, acquisition matrix 384 × 186, and slice thickness 4 mm.

2.5. MRI data analysis

2.5.1. Gray matter analyses

A multimodal approach was implemented to comprehensively characterize mesial temporal lobe pathology in the 3 study groups. Total hippocampal volumes were estimated, hippocampal segmentation was performed to estimate volumes of specific subfields, vertex analyses were undertaken to reflect on shape deformation, and supplementary brain morphometry was carried out to confirm disease-specific cerebral gray matter signatures.

Table 1
The demographic and clinical profile of study participants

	ALS (n = 50)	AD (n = 18)	HC (n = 40)	Statistical differences
Age (years)	61.70 ± 10.22	76.28 ± 6.37	59.00 ± 6.28	AD>HC ($p < 0.001$) AD>ALS ($p < 0.001$)
Gender (M/F)	28/22	2/16	18/22	AD vs. HC ($p = 0.012$), AD vs. ALS ($p = 0.001$)
Education (years)	10.62 ± 3.53	7.89 ± 5.06	14.00 ± 2.43	HC>ALS, AD ($p < 0.001$) ALS>AD ($p = 0.014$)
Handedness (Rt/Lt)	50/0	18/0	40/0	Ns
Disease duration from symptom onset (m)	17.72 ± 18.34	33.67 ± 21.60	–	ALS<AD ($p = 0.004$)
ALSFRS-R	39.80 ± 6.10	–	–	–
ALS onset (S/B)	38/12	–	–	–
Riluzole (Y/N)	14/36			
MMSE	26.08 ± 2.22	23.00 ± 3.07	28.50 ± 1.06	HC>ALS, AD ($p < 0.001$) ALS>AD ($p = 0.001$)

Differences in MMSE are adjusted for age, gender, and education.
Key: AD, Alzheimer's dementia; ALS, amyotrophic lateral sclerosis; ALSFRS-R, Amyotrophic Lateral Sclerosis Functional Rating Scale-revised; HC, healthy controls; M/F, male/female; m, months; MMSE, Mini–Mental State Examination; Rt/Lt, right/left; S/B, spinal/bulbar; Y/N, yes/no.

Table 2
Memory profile of the ALS groups and ALS-high and ALS-low subgroups

	ALS		ALS-high		ALS-low	
	Raw	Z-score	Raw	Z-score	Raw	Z-score
RAVLT-Learning	38.44 ± 9.03	−0.49 ± 1.95	46.22 ± 5.97	0.67 ± 1.84	31.81 ± 4.94	−1.47 ± 1.45
RAVLT-IR	7.14 ± 3.00	−0.34 ± 2.98	9.35 ± 2.27	1.36 ± 2.54	5.26 ± 2.16	−1.79 ± 2.55
RAVLT-DR	5.84 ± 2.96	−1.86 ± 3.15	7.48 ± 2.71	−0.76 ± 3.06	4.44 ± 2.49	−2.79 ± 2.96
BSRT-IR	10.02 ± 2.17	−0.82 ± 1.22	10.87 ± 2.24	−0.56 ± 1.32	9.30 ± 1.86	−1.03 ± 1.11
BSRT-DR	8.22 ± 3.50	−1.53 ± 1.78	9.96 ± 3.88	−0.81 ± 1.91	6.74 ± 2.31	−2.14 ± 1.43
ROCFT-IR[a]	13.32 ± 6.11	−0.69 ± 1.17	16.56 ± 5.94	−0.25 ± 1.16	10.86 ± 5.09	−1.02 ± 1.08

Z-scores were calculated based on available normative data (Messinis et al., 2007; Meyers and Meyers, 1995; Zalonis et al., 2008).
Key: ALS, amyotrophic lateral sclerosis; BSRT, Babcock Story Recall Test; DR, Delayed Recall; IR, Immediate Recall; ROCFT, Rey-Osterrieth Complex Figure Test; RAVLT, Rey Auditory Verbal Learning Test.
[a] Available for 16 ALS-high and 21 ALS-low performers.

First, total intracranial volume (TIV) was estimated for each participant to be used as a covariate for volumetric analyses. TIV was estimated by linearly aligning each subject's skull-stripped brain to the standard MNI152 brain image in MNI space, calculating the inverse of the determinant of the affine registration matrix and multiplying it by the size of the template. Registration to template was undertaken using FMRIB's model-based registration tool (Jenkinson and Smith, 2001), and FMRIB's automated segmentation tool was used for tissue-type segmentation (Zhang et al., 2001).

The hippocampus was segmented into cytologically defined subfields (Fig. 1A) using the FreeSurfer image analysis suite, version 6.0 (Fischl, 2012). The preprocessing pipeline included the removal of nonbrain tissue, segmentation of the subcortical white matter and deep gray matter structures, intensity normalization, tessellation of the gray matter–white matter boundary, and automated topology correction. The hippocampal stream of the FreeSurfer package was used for the accurate segmentation of the following hippocampal subfields: CA1, CA2/3, CA4, fimbria, hippocampal fissure, presubiculum, subiculum, hippocampal tail, parasubiculum, molecular layer; granule cell layer of the dentate gyrus (GC-DG), hippocampus-amygdala transition area (HATA) (Iglesias et al., 2015).

Vertex analyses were performed using FMRIB's subcortical segmentation and registration tool FIRST to provide quantitative, surface-projected information about focal hippocampal involvement. Vertex locations of individual subjects were projected on the surface of an average template shape as scalar values, positive value being outside the surface and negative values inside. Design matrices included age, gender, and education.

To confirm disease-specific gray matter signatures beyond the hippocampus, supplementary morphometric analyses were carried out in the FSL environment (Smith et al., 2004). Following brain extraction and tissue-type segmentation, gray matter partial volume images were aligned to the MNI152 standard space using affine registration (Good et al., 2001). The resulting images were averaged and flipped along the x-axis to create a left-right symmetric, study-specific gray matter template. All native gray matter images were nonlinearly coregistered to the study-specific template, modulated by a Jacobian field warp and smoothed with an isotropic gaussian kernel with a sigma of 3 mm. The threshold-free cluster-enhancement method (Smith and Nichols, 2009) and permutation-based nonparametric inference were used for the comparison of study groups controlling for age, gender, and education.

2.5.2. White matter analyses

White matter tractography was conducted using Brainance DTI Suite (Advantis Medical Imaging, Eindhoven, The Netherlands). First, the raw DWI data sets were motion and eddy current

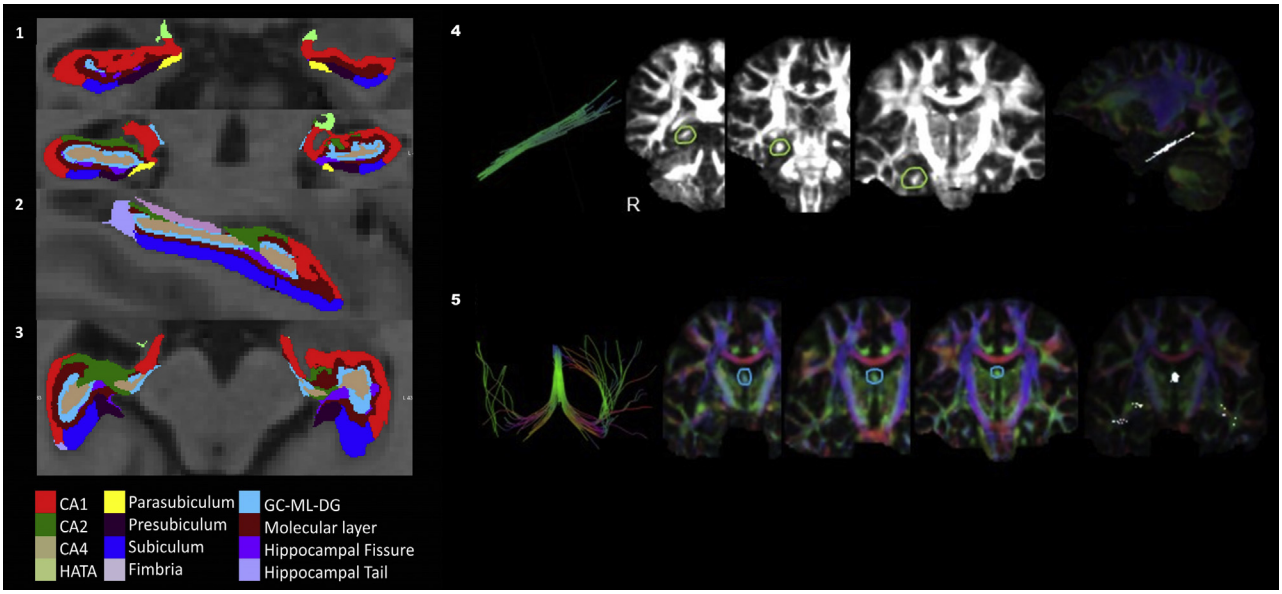

Fig. 1. Left: Hippocampal segmentation and resulting subfields in coronal (1), sagittal (2), and axial views (3) Right: The tractographic reconstruction of the right perforant pathway (4) and the fornix (5) with their respective region-of-interest gates on fractional anisotropy maps.

Table 3
Volumes of specific hippocampal subfields and the entire hippocampus—the white matter profile of the PPZ and the fornix in ALS, AD, and HC

	HC (N = 40)	ALS (N = 50)	AD (N = 18)	ALS-high (N = 23)	ALS-low (N = 27)	ALS vs. HC	ALS vs. AD	AD vs. HC	ALS-high vs. HC	ALS-high vs. ALS-low	ALS-low vs. AD
	Mean ± SD					*p*-values					
Total hippocampal volumes											
Left	3423.84 ± 422.85	3223.46 ± 458.38	2415.54 ± 342.73	3305.07 ± 396.81	3153.95 ± 501.84		**<0.001**	**<0.001**			**<0.001**
Right	3506.29 ± 444.01	3308.92 ± 446.37	2542.70 ± 393.01	3412.04 ± 396.29	3221.09 ± 474.55		**<0.001**	**<0.001**		**0.018**	**<0.001**
Subfields in the left hemisphere											
CA1	632.03 ± 91.25	594.36 ± 97.22	467.90 ± 73.10	607.49 ± 98.07	583.17 ± 96.91		**<0.001**	**<0.001**			**0.016**
CA2/CA3	202.25 ± 28.90	189.14 ± 33.09	143.51 ± 27.90	187.66 ± 21.51	190.40 ± 40.85	**0.049**	**<0.001**	**<0.001**			**0.005**
CA4	251.70 ± 31.25	237.39 ± 35.51	176.04 ± 30.25	240.23 ± 27.62	234.97 ± 41.44		**<0.001**	**<0.001**			**0.001**
Fimbria	72.98 ± 12.41	61.73 ± 19.64	34.67 ± 10.65	69.27 ± 19.77	55.31 ± 17.40	**0.007**	**0.002**	**<0.001**		**0.013**	**0.037**
Hippocampal fissure	150.35 ± 27.08	178.57 ± 35.13	169.57 ± 37.40	172.17 ± 40.14	184.02 ± 29.93	**<0.001**	**0.040**		**0.013**		
Presubiculum	313.52 ± 47.34	299.03 ± 47.62	219.01 ± 32.57	303.36 ± 42.99	295.35 ± 51.76		**<0.001**	**<0.001**			**0.001**
Subiculum	448.95 ± 61.43	425.82 ± 62.08	310.31 ± 48.79	434.56 ± 55.44	418.37 ± 67.31		**<0.001**	**<0.001**			**0.001**
Hippocampal tail	520.62 ± 74.85	508.34 ± 89.37	390.52 ± 55.91	535.10 ± 78.09	485.54 ± 93.37		**0.010**			**0.035**	
Parasubiculum	56.33 ± 12.56	53.37 ± 13.65	48.58 ± 9.48	51.10 ± 10.37	55.31 ± 15.86						
Molecular layer	571.55 ± 73.67	531.82 ± 81.33	388.06 ± 59.30	546.62 ± 72.15	519.22 ± 87.77	**0.020**	**<0.001**	**<0.001**			**0.001**
GC-DG	293.12 ± 37.40	270.44 ± 42.22	194.88 ± 32.86	276.19 ± 33.44	265.54 ± 48.56	**0.021**	**<0.001**	**<0.001**			**0.001**
HATA	60.77 ± 11.94	52.02 ± 8.52	42.07 ± 5.10	53.49 ± 7.84	50.76 ± 9.01	**<0.001**		**0.002**	**0.016**		
Subfields in the right hemisphere											
CA1	648.04 ± 92.79	618.67 ± 84.67	489.56 ± 83.20	639.21 ± 80.30	601.18 ± 85.81		**<0.001**	**<0.001**		**0.041**	**0.005**
CA2/CA3	224.59 ± 36.50	207.10 ± 35.01	164.06 ± 28.12	211.76 ± 31.46	203.14 ± 37.91	**0.026**	**0.006**	**<0.001**			**0.041**
CA4	265.54 ± 35.90	249.90 ± 36.22	197.82 ± 32.50	256.37 ± 32.21	244.40 ± 39.06		**<0.001**	**<0.001**			**0.005**
Fimbria	70.31 ± 15.10	63.92 ± 20.17	40.05 ± 16.89	69.91 ± 18.28	58.82 ± 20.62		**0.021**	**0.009**			
Hippocampal fissure	162.18 ± 29.38	191.63 ± 36.39	180.33 ± 42.81	182.63 ± 37.29	199.30 ± 34.45	**<0.001**	**0.002**		**0.026**		**0.001**
Presubiculum	298.44 ± 42.44	283.27 ± 47.40	211.78 ± 39.68	287.14 ± 47.40	279.97 ± 48.05		**<0.001**	**<0.001**			**0.001**
Subiculum	443.93 ± 59.09	426.36 ± 62.48	319.66 ± 58.91	434.01 ± 53.34	419.84 ± 69.66		**<0.001**	**<0.001**			**0.001**
Hippocampal tail	545.56 ± 74.13	518.59 ± 84.42	400.22 ± 60.40	542.76 ± 77.47	498.01 ± 85.99		**0.002**			**0.026**	**0.036**
Parasubiculum	55.57 ± 12.31	53.54 ± 13.82	43.53 ± 8.99	51.63 ± 12.94	55.16 ± 14.56						
Molecular layer	584.41 ± 76.96	544.43 ± 76.24	408.41 ± 69.53	563.54 ± 66.92	528.15 ± 81.04	**0.020**	**<0.001**	**<0.001**		**0.026**	**0.001**
GC-DG	307.73 ± 41.36	286.59 ± 43.15	221.56 ± 39.13	296.41 ± 37.63	278.22 ± 46.40		**<0.001**	**<0.001**		**0.041**	**0.005**
HATA	62.17 ± 9.84	56.55 ± 11.34	46.05 ± 8.83	59.29 ± 9.40	54.22 ± 12.46			**0.013**			
White matter tract DTI metrics											
Lt Hippocampal PPZ											
FA	0.39 ± 0.02	0.39 ± 0.02	0.39 ± 0.02	0.40 ± 0.02	0.39 ± 0.02						
Dax ($\times 10^{-3}$)	1.18 ± 0.05	1.19 ± 0.04	1.25 ± 0.05	1.19 ± 0.04	1.18 ± 0.05		**<0.001**	**<0.001**			**0.001**
Drad ($\times 10^{-3}$)	0.63 ± 0.03	0.63 ± 0.03	0.68 ± 0.04	0.63 ± 0.03	0.63 ± 0.03		**<0.001**	**<0.001**			**0.001**
Rt Hippocampal PPZ											
FA	0.40 ± 0.02	0.39 ± 0.02	0.38 ± 0.02	0.39 ± 0.02	0.39 ± 0.03						
Dax ($\times 10^{-3}$)	1.16 ± 0.05	1.19 ± 0.05	1.29 ± 0.09	1.18 ± 0.05	1.19 ± 0.06	**0.024**	**<0.001**	**<0.001**			**0.005**
Drad ($\times 10^{-3}$)	0.61 ± 0.003	0.63 ± 0.04	0.71 ± 0.06	0.63 ± 0.03	0.64 ± 0.04		**<0.001**	**<0.001**			**0.005**
Fornix											
FA	0.37 ± 0.02	0.35 ± 0.04	0.30 ± 0.04	0.36 ± 0.03	0.34 ± 0.04	**0.036**	**0.008**	**<0.001**			**0.042**
Dax ($\times 10^{-3}$)	1.92 ± 0.01	2.04 ± 0.02	2.28 ± 0.02	1.97 ± 0.02	2.09 ± 0.02	**0.002**	**0.002**	**<0.001**			**0.027**
Drad ($\times 10^{-3}$)	1.10 ± 0.09	1.21 ± 0.02	1.47 ± 0.02	1.16 ± 0.01	1.26 ± 0.02	**0.004**	**<0.001**	**<0.001**			**0.005**

Absolute hippocampal subfields volumes (mm^3) and DTI metrics (FA, Dax, Drad) are presented for each group. Age, gender, education, and TIV (for hippocampal subfields) were used as covariates in the MANCOVA analyses. n/a: post hoc comparisons were not conducted due to nonsignificant ($p > 0.05$) F-test. Bold post hoc comparisons are significant after false discovery rate correction for multiple comparisons.
Key: AD, Alzheimer's disease; ALS, amyotrophic lateral sclerosis; CA, cornu ammonis; Dax, axial diffusivity; Drad, radial diffusivity; DTI, diffusion tensor imaging; FA, fractional anisotropy; GC-DG, granule cell layer of dentate gyrus; HATA, hippocampus-amygdala transition area; HC, healthy controls; Lt/Rt, left/right; PPZ, perforant pathway zone; SD, standard deviation; WM, white matter.

corrected. Three regions of interest were used for the reconstruction of the perforant pathway zone (PPZ); (1) on a coronal slice at the middle of the splenium of the corpus callosum, the perforant pathway was identified subjacent the corpus callosum, (2) on a coronal slice anterior to the first one at the level of the cerebellar dentate nucleus, and (3) the white matter area of the mesial temporal lobe just underlying the hippocampus on a coronal slice anterior to the pons at the level where the projections of the posterior limb of internal capsule are prominent (Fig. 1B). For the reconstruction of the fornix, 3 regions of interest were placed along the fornix in 3 coronal slices where the fornix was visible as one bundle (Fig. 1C). The following parameters were used for tracking—PPZ: fractional anisotropy (FA) threshold 0.20 and angle threshold 6; and fornix: FA threshold 0.25 and angle threshold 60. To provide a multifaceted characterization of white matter integrity changes, the following diffusivity metrics were extracted for each tract: FA, axial diffusivity (Dax), and radial diffusivity (Drad). Intra- and inter-rater reliability were assessed for all tracts in each participant and showed high intra-class correlation (ICC $>$ 0.8).

2.6. Statistical analyses

Assumptions of normality were examined using the Kolmogorov-Smirnov test. Because all variables followed a normal distribution, parametric statistics were applied. Considering the patients' heterogeneous memory performance, a hierarchical cluster analysis using Ward's method of minimum variance with a squared Euclidean distance measure was conducted within the ALS cohort to identify clusters of memory performance (i.e., "ALS-high performers" and "ALS-low performers") based on episodic memory measures (i.e., Rey Auditory Verbal Learning Test—Total Learning, Immediate Recall, and Delayed Recall; Babcock Story Recall Test—Immediate Recall and Delayed Recall). Ward's method was chosen because of its efficiency to model quantitative variables and its resilience to outlier effects. The squared Euclidean distance coefficient was calculated as it is the most widely used distance coefficient in neuropsychological studies and detects performance levels and patterns within the clusters (Allen and Goldstein, 2013). The following multivariate analyses of covariance (MANCOVAs) were conducted to examine differences in hippocampal subfields and tractography measures (1) HC, ALS, and AD and (2) HC, ALS-high, ALS-low, and AD using age, gender, education, and TIV (for subfield volumes) as covariates. If a significant main effect of group membership was found ($p < 0.05$), post hoc group comparisons were performed using the false discovery rate (FDR) correction for multiple comparisons. Correlation analyses (Pearson r) were also conducted within the ALS group between MRI metrics and patients' clinical data. The significance level was set at $p < 0.05$.

3. Results

3.1. The volumetric profile of hippocampal subfields

The adjusted estimated marginal means and standard error of hippocampal subfield volumes are presented in Table 3. Significant differences were observed in total hippocampal volumes between the ALS and AD ($p < 0.001$) and between HCs and AD ($p < 0.001$). Significant main effects of group were observed for all subfields with the exception of the parasubiculum. Compared with HCs, patients with ALS showed significant volume reductions in the bilateral CA2/3, left fimbria, bilateral molecular layer, left GC-DG, left HATA, and increased bilateral hippocampal fissure volumes. Compared with AD patients, patients with ALS showed higher volumes in all CA subfields, fimbria, presubiculum and subiculum, hippocampal tail, molecular layer, GC-DG, and hippocampal fissure. With the exception of the hippocampal fissures and hippocampal tail, the AD group exhibited widespread hippocampal atrophy in all hippocampal subfields compared with HCs.

Regarding the neuropsychologically defined ALS subgroups, no significant hippocampal volume differences were identified between HCs and ALS-high. ALS-low performers showed significantly reduced volume in the right hippocampus compared with ALS-high ($p = 0.018$) and higher volume bilaterally compared with AD ($p < 0.001$). With regard to hippocampal subfields, the ALS-high cohort exhibited higher bilateral hippocampal fissure volumes (left: $p = 0.013$; right: $p = 0.026$) and decreased left HATA volumes ($p = 0.016$) compared with HCs. The direct comparison on subfields between the 2 ALS groups revealed volume reductions in the ALS-

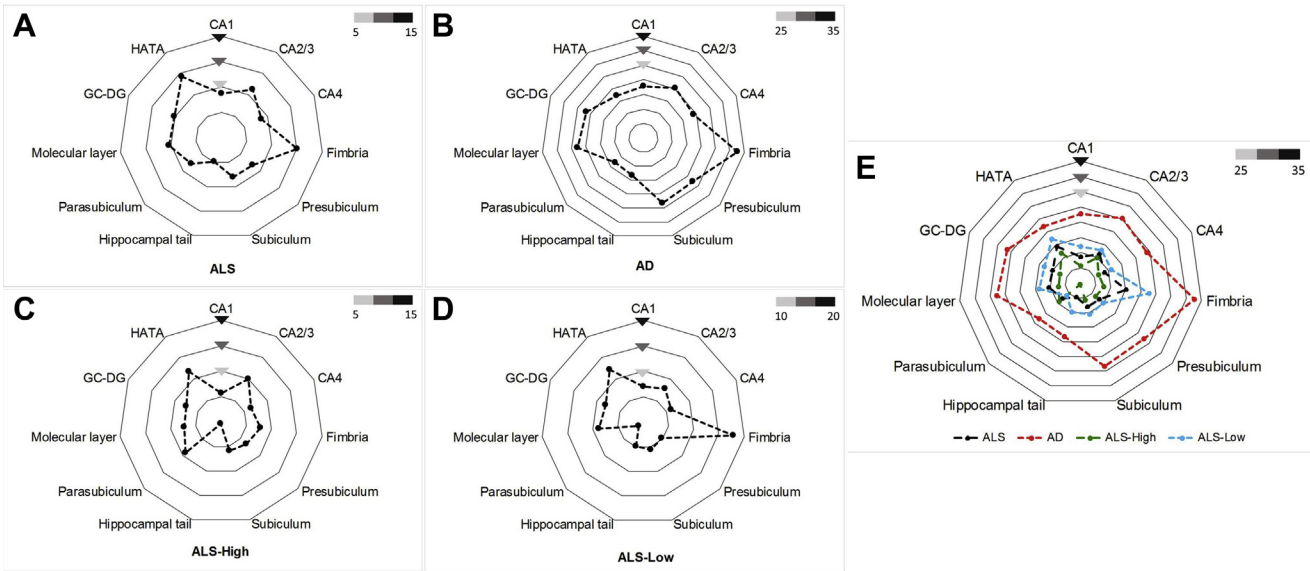

Fig. 2. The regional hippocampal profile of each study group: ALS (A), AD (B), ALS-high (C) and ALS-low (D), and their comparative volumetric profile (E) with reference to healthy controls/subfield volumes are averaged across left and right. Abbreviations: AD, Alzheimer's disease; ALS, amyotrophic lateral sclerosis; CA, cornu ammonis; HATA, hippocampus-amygdala transition area; HCs, healthy controls; GC-DG, granule cell layer of dentate gyrus.

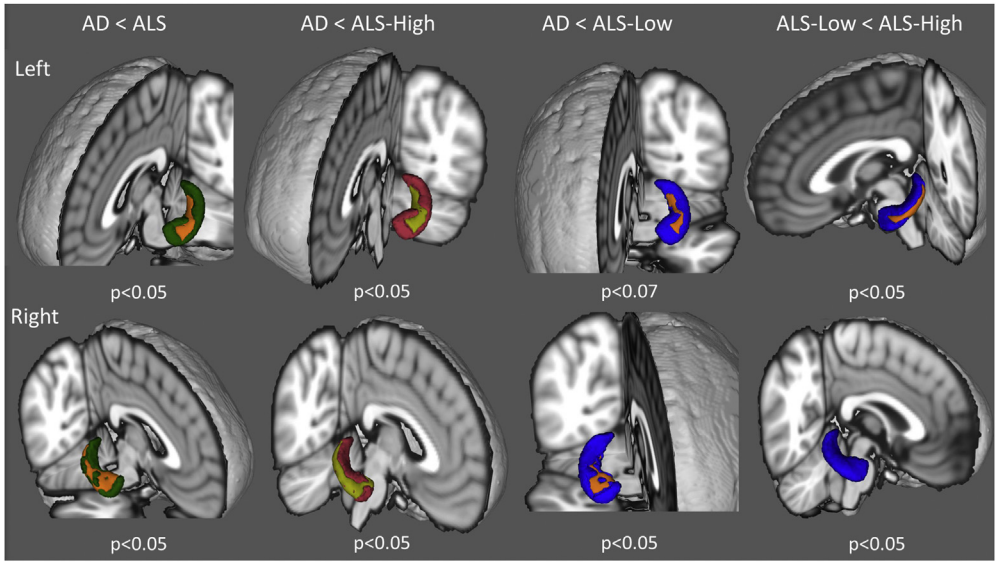

Fig. 3. The comparative hippocampal atrophy profile of the AD, ALS-high, and ALS-low cohorts. Surface projected patterns of atrophy are highlighted in orange and yellow, and the underlying hippocampal mesh volumes are represented in green, pink, and blue. Comparisons are adjusted for age, gender, and education. Abbreviations: AD, Alzheimer's disease; ALS, amyotrophic lateral sclerosis. (For interpretation of the references to color in this figure legend, the reader is referred to the Web version of this article.)

low group in the left fimbria, bilateral hippocampal tails, right CA1, right molecular layer, and right GC-DG.

The most affected hippocampal subfields in the study groups were identified using percentage of change with reference to HCs and averaging left and right volumes of respective subfields. Fig. 2 illustrates the hippocampal profile of the study groups using estimated marginal means adjusted for age, gender, education, and TIV. Based on normative reference values, the HATA and CA2/3 are the most affected subfields in ALS, the presubiculum and subiculum in AD, and the fimbria are affected in both ALS and AD. In the neuropsychologically defined ALS groups, the fimbria and HATA are particularly atrophic in the ALS-low group and HATA and CA2/3 are the most affected subfields in the ALS-high cohort.

3.2. Vertex analyses

Vertex analyses demonstrated that the inferior and superior aspects of both left and right hippocampi are more affected in AD than ALS. No significant differences were identified between ALS-high performers and HCs. Compared with ALS-low performers, the AD group revealed considerable surface-projected atrophy in the right hippocampus at $p < 0.05$ and a trend of atrophy at $p < 0.07$ in the left hippocampus (Fig. 3). The contrast between the neuropsychologically defined ALS-high and ALS-low groups also revealed significant shape differences in the lateral aspect of the left hippocampus.

3.3. Whole-brain morphometric analyses

Our voxel-based morphometry-type analyses confirmed disease-associated cerebral signatures. The AD group exhibited widespread bitemporal and biparietal atrophies, whereas the ALS cohort showed degenerative changes in the bilateral motor cortices (Fig. 4).

3.4. DTI metrics

The adjusted estimated marginal means of white matter tracts for HCs, ALS, and AD are summarized in Table 3. No significant group effect was identified for FA values in bilateral PPZ. Compared

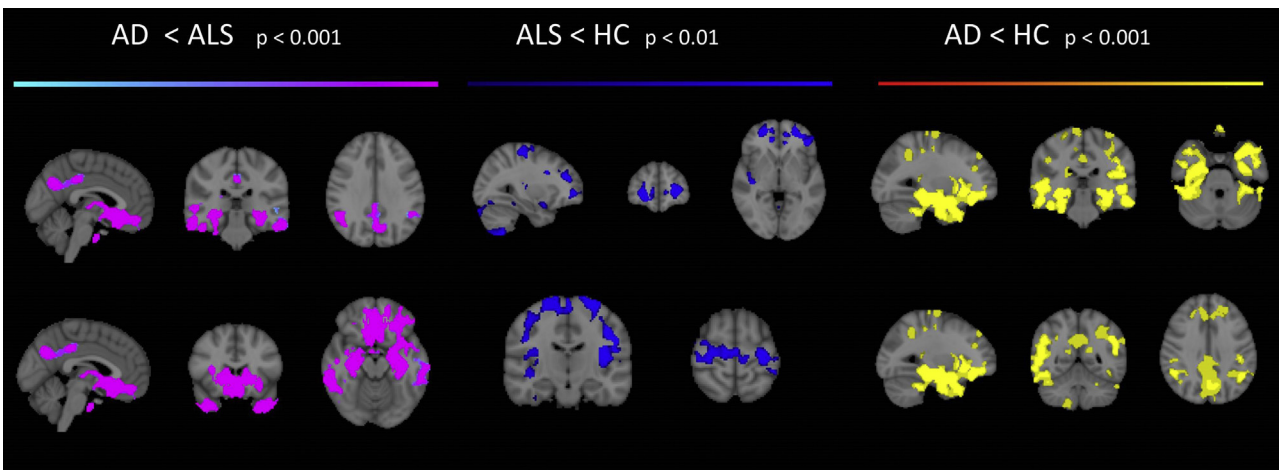

Fig. 4. Cortical atrophy patterns in ALS and AD identified by voxel-based morphometry using age, gender, and education as covariates. Abbreviations: AD, Alzheimer's disease; ALS, amyotrophic lateral sclerosis; HC, healthy control.

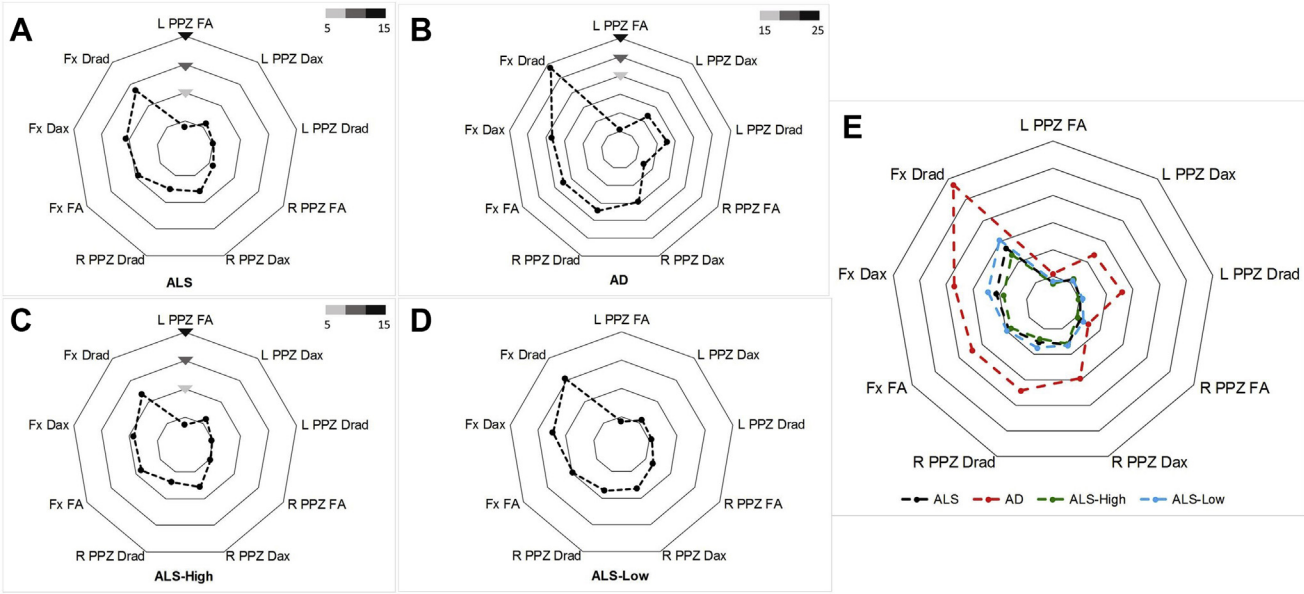

Fig. 5. The diffusivity profile of the perforant pathway and fornix in each study group: ALS (A), AD (B), ALS-high (C) and ALS-low (D), and their comparative profile (E) with reference to healthy controls. Abbreviations: AD, Alzheimer's disease; ALS, amyotrophic lateral sclerosis; Dax, axial diffusivity; Drad, radial diffusivity; Fx, fornix; FA, fractional anisotropy; HCs, healthy controls; L, left; PPZ, perforant pathway zone; R, right.

with HCs, patients with ALS exhibit significantly lower FA in fornix, higher Dax in right PPZ, and higher Dax and Drad in fornix. Compared with AD, ALS patients also exhibited significantly higher FA in the fornix, and lower Dax and Drad in the bilateral PPZ and fornix. The comparison between HCs and AD confirmed widespread white matter pathology in both the PPZ and fornix.

The direct comparison of DTI metrics in ALS-high and ALS-low performers did not reach statistical significance using FDR corrections. Compared with AD patients, ALS-low performers exhibited higher FA in the fornix and lower Dax and Drad in both the PPZ and fornix.

Fig. 5 depicts the DTI profile of the PPZ and fornix in ALS, AD, ALS-high, and ALS-low performers with reference to HCs. Fornix (specifically on Drad) was the most affected tract in both ALS and AD. Drad and Dax indices of the right PPZ were the second most affected metrics in the study groups.

3.5. Correlation with clinical and memory variables

To avoid type II error, correlation analyses were restricted to imaging metrics showing significant differences between HCs and ALS. Following correction for multiple comparisons, neither disease duration, revised ALS Functional Rating Scale, nor memory scores correlated with gray or white matter metrics.

4. Discussion

Our findings indicate that ALS is associated with widespread hippocampal pathology, which is independent of disease duration and motor disability and is distinct from AD. The novelty of our study lies in the integration of gray and white matter metrics and the ascertainment of divergent hippocampal signatures in ALS and AD.

4.1. Radiological insights into hippocampal pathology in ALS and AD

There is ample pathological evidence of hippocampal pathology in ALS, but the neuroimaging literature is relatively sparse (Christidi et al., 2018b). Hippocampal atrophy has been demonstrated in both *C9orf72*-negative and *C9orf72*-positive ALS patients (Bede et al., 2013b; Floeter et al., 2018) and is not due to the inclusion of patients with comorbid frontotemporal dementia (Abdulla et al., 2014; Westeneng et al., 2015). The majority of existing MRI studies in ALS evaluate entire hippocampal volumes and rely on HCs alone as opposed to disease controls (Abdulla et al., 2014; Bede et al., 2013b; Bueno et al., 2018; Christidi et al., 2018b; Machts et al., 2018; Westeneng et al., 2015). We identified selective subfield involvement in ALS in bilateral CA2/CA3 and left fimbria, with the relative sparing of the subiculum and presubiculum. A more widespread anatomical pattern of hippocampal change was identified in AD with the preferential involvement of the subiculum and presubiculum. The independence of hippocampal pathology from motor disability is an important finding, as clinical trials of ALS continue to overwhelmingly rely on motor metrics (Mitsumoto et al., 2014) despite evidence of considerable disease burden in nonmotor regions (Christidi et al., 2018a). Hippocampal subfields are routinely assessed in studies of normal aging, mild cognitive impairment and AD (de Flores et al., 2015) but seldom evaluated in ALS (Westeneng et al., 2015). Our findings highlight the utility of subfield analyses versus whole-hippocampal volumetry and underline the selective vulnerability of specific subfields, with distinct cytoarchitecture, dedicated functions, and distinct connections (Duvernoy et al., 2013). The entire ALS group, irrespective of neuropsychological performance, exhibited hippocampal atrophy. Following the stratification of ALS patients based on memory performance, vertexwise and volumetric differences were identified between ALS-high and ALS-low performers underscoring the detection sensitivity of neuropsychological tests to capture hippocampal pathology.

The most affected subfields in ALS are CA2/CA3 and HATA, the presubiculum and subiculum in AD, and the fimbria in both groups. Fimbria is a white matter subfield, which runs along the superomedial edge of the hippocampus and then at the posterior part of the hippocampus and transitions into the crux of the fornix. Fimbria and HATA have not been previously studied in ALS as a distinct hippocampal subfield due to the methodological constraints of

older segmentation approaches (Westeneng et al., 2015). The involvement of the fimbria in ALS, particularly its atrophy in the ALS-low cohort, is in line with its role (Zheng et al., 2018) in memory function and consistent with previous studies suggesting that fornix metrics may indicate AD risk in cognitively normal persons and may also act as prognostic indicators for conversion from mild cognitive impairment and AD (Nowrangi and Rosenberg, 2015).

Our findings also need to be discussed from a "tau" versus "TAR DNA-binding protein 43 (TDP-43)" perspective. The AD cohort in this study is likely to represent a relatively homogenous group pathologically as they had no evidence motor involvement and their voxel-based morphometry analysis confirmed disease-specific bitemporal and biparietal pathology and fulfilled clinical criteria, therefore representing an archetypic AD cohort without clinical and radiological features suggestive of TDP. The hippocampal imaging signature of our AD cohort is also consistent with larger imaging studies (Evans et al., 2018). Conversely, our ALS cohort is less likely to be pathologically homogenous and may include patients with coexisting tau pathology (Frecker et al., 1990; Segers et al., 2012). Thus, fimbria changes detected in the ALS cohort may, in part, be manifestations of coexisting AD pathology.

4.2. Network-wise degeneration in ALS

Our study demonstrates the benefit of using multiple complementary imaging techniques and systematically evaluating gray and white matter structures (Bede and Hardiman, 2014). Subfield volumetrics and shape analysis provided complementary insights; vertex analyses captured differences between ALS-high and ALS-low performers, whereas subfield volumetrics revealed selective hippocampal vulnerability. The selective degeneration of cell-specific hippocampal regions is also well recognized in healthy aging (Haigler et al., 1986).

An additional advantage of appraising multiple gray and white matter metrics is the establishment of their respective sensitivity profiles. From a motor perspective, corticospinal white matter degeneration is invariably detected irrespective of disease duration (Bede and Hardiman, 2018; Pyra et al., 2010), but the detection of cortical gray matter involvement depends on disease stage, upper motor neuron predominance, and imaging techniques (Bede et al., 2013a). In contrast, our study indicates that hippocampal gray matter metrics (subfields volumes and vertex metrics) readily detect mesial temporal lobe pathology. The ranking of the detection sensitivity of various imaging metrics is indispensable to establish which index may be used in diagnostic, monitoring, or prognostic applications (Schuster et al., 2015, 2017).

Our findings also confirm the concomitant degeneration of associated gray and white matter structures in ALS (Bede et al., 2018a; Nasseroleslami et al., 2017). The fimbria was the most affected hippocampal subfield in both ALS and AD, which is consistent with the widespread diffusivity changes identified in the fornix. The perforant pathway linking the entorhinal cortex, dentate gyrus, CA, and subiculum is preferentially affected in our AD cohort, which is consistent with the selective degenerative changes observed in the hippocampal subfields it connects. The evaluation of multiple diffusivity metrics helps the biological characterization of white matter degeneration. Although FA is widely regarded a composite proxy of white matter integrity, Dax is primarily regarded as an axonal marker and Drad also reflects on myelin-related pathology (Song et al., 2005; Sun et al., 2006).

4.3. Pathological correlates

The lack of correlations between clinical measures and radiological findings do not directly support a sequential model of pathological spread in ALS and highlight a possible inconsistency between radiological observations and the pathological staging. In ALS, pathological TDP-43 can be detected in the hippocampal CA4-CA1/subiculum in 25% of postmortem samples (Geser et al., 2008). Pathological TDP-43 burden in the anteromedial temporal lobe and the hippocampal formation are now regarded as a stage-defining feature of a widely used pathological staging system in ALS (Brettschneider et al., 2013), corresponding to "stage 4" of the disease.

According to the 3-stage model of PPZ degeneration, stage I ("inclusion stage") is characterized by TDP-43-positive cytoplasmic inclusions in the granular cells of the dentate gyrus, stage II (i.e., "early perforant stage") by gliosis and neuronal loss in the transentorhinal cortex, and stage III (i.e., "advanced perforant stage") by the degeneration of the molecular layer of the dentate gyrus (Takeda et al., 2009). These stages of hippocampal pathology are closely linked to its white matter architecture, suggestive of connectivity-based disease propagation (Schmidt et al., 2016) and supports the notion that interconnected gray matter regions become gradually affected as opposed to contiguous spread (Braak et al., 2013). As certain hippocampal subfields, such as the subiculum, remain unaffected in our ALS cohort, our findings also support the concept of network-wise propagation as opposed to the contiguous involvement of adjacent structures.

4.4. Clinical relevance

Our findings may have implications for caregiver support, screening strategies, and clinical trial designs. Memory impairment in ALS remains relatively under-recognized despite its quality-of-life implications and potential effect on compliance with assistive devices, engagement in rehabilitation efforts, and participation in clinical trials (Lomen-Hoerth et al., 2003; Olney et al., 2005). Pharmacological studies of ALS continue to rely on survival and clinical scores as key outcome measures overlooking the biomarker potential of quantitative neuroimaging measures, which are widely used in studies of other neurological disorders (Chipika et al., 2019). Furthermore, current clinical trials overwhelmingly focus on mobility, motor deficits, and respiratory dysfunction as endpoints despite irrefutable evidence of widespread extra-motor involvement in ALS (Beeldman et al., 2016; Christidi et al., 2018a). Frontotemporal involvement is a key contributor to clinical heterogeneity in ALS; it has survival (Elamin et al., 2011; Ishaque et al., 2018) and caregiver burden implications (Caga et al., 2018), yet it is not evaluated in most clinical trials. At a time when ALS-specific cognitive instruments have been extensively validated (Abrahams et al., 2014) and noninvasive neuroimaging techniques readily capture motor and extra-motor changes, the incorporation of cognitive testing and quantitative imaging protocols into pharmacological trials seems overdue.

4.5. Study limitations and future directions

This study is not without limitations. The biggest shortcoming of this report is the small sample size of our AD group, which was included as a disease control group. Despite the sample size limitation of the AD cohort, this group exhibits disease-associated atrophy patterns typical of AD. Owing to disease-specific characteristics, the AD cohort of our study is older than the ALS patients and healthy controls included in our imaging analyses.

Although age was strictly included as a covariate in all of our statistical models, to ensure that age differences have not influenced our findings, an additional subanalysis was conducted with an age-matched ($p = 0.135$), education-matched ($p = 0.078$), and gender-matched ($p = 0.334$) subcohort of AD patients and controls. The structural differences identified by this age-matched supplementary analysis were consistent with our main findings indicating that the identified hippocampal patterns are disease related and not driven by age. This study focused on ALS, but as relatively little is known of the hippocampal profile of other motor neuron disease phenotypes, the inclusion of additional "disease controls," such as primary lateral sclerosis (Finegan et al., 2019a), Kennedy's disease, or spinal muscular atrophy patients would have potentially contributed important additional insights (Finegan et al., 2019c; Querin et al., 2018, 2019). Our choice of a 2-cluster model to stratify our ALS cohort for memory performance was also driven by sample size considerations. Another potential limitation of our study is the risk of partial volume effects on the tractographic reconstruction of the fornix. CSF contamination however typically affects axial and radial diffusivity metrics, and FA is thought to be less influenced by it (Douet and Chang, 2014). Dedicated acquisition methods (Baron and Beaulieu, 2015) and postprocessing approaches (Chad et al., 2018; Metzler-Baddeley et al., 2012) would be required if the primary focus of the study would be the characterization of fornix integrity. Our fornix findings however are in line with previous studies of ALS and AD and consistent with recent reports in neuropsychologically unaffected subjects with elevated Aβ burden (Rabin et al., 2019). An additional drawback of the study is the lack of comprehensive genetic profiling to explore whether *C9orf72* hexanucleotide repeats may contribute to the hippocampal disease burden observed in this study. However, the potential influence of *C9orf72* hexanucleotide carriers in our sample is not considered substantive because our sample only included sporadic ALS cases, and the prevalence of *C9orf72* hexanucleotide carriers in the Greek population is 8% in sporadic cases (Mok et al., 2012). Previous studies indicate that *C9orf72*-negative ALS patients exhibit overall hippocampal pathology (Machts et al., 2015), which may be more marked in hexanucleotide carriers (Bede et al., 2013b). Finally, spinal fluid panels for tau, amyloid, and neurofilaments in the ALS cohort would have provided important additional insights to reflect on the molecular substrate of hippocampal pathology. Notwithstanding these limitations, our study demonstrates the divergent mesial temporal lobe profile of ALS and AD, highlighting the need for further wet-biomarker-supported and histopathologically validated studies. Emerging imaging modalities such as neurite orientation dispersion and density imaging (Barritt et al., 2018) and high-field MR imaging (Cardenas et al., 2017) may help to characterize mesial temporal lobe degeneration in ALS further.

5. Conclusions

Patients with ALS exhibit disease-specific patterns of hippocampal pathology, which is distinct from AD. The preferential involvement of specific hippocampal subfields connected by selectively affected white matter projections suggests network-based disease propagation as opposed to contagious spread. The comprehensive characterization of mesial temporal lobe degeneration in ALS has implications for screening practices, supportive interventions, clinical trial designs, and expanding the extra-motor profile of ALS.

Disclosure

The authors have no actual or potential conflicts of interest.

Acknowledgements

We acknowledge the generosity and kindness of our patients for participating in the ALS imaging studies worldwide.

Foteini Christidi is supported by the State Scholarships Foundation (I.K.Y.; Postdoctoral Support, Greece; EP ANADEDBM/ESPA, 2014–2020). Peter Bede is supported by the Health Research Board (HRB–Ireland; HRB EIA-2017-019), the Andrew Lydon scholarship, the Irish Institute of Clinical Neuroscience (IICN) Research Grant, the Iris O'Brien Foundation, the Research Motor Neuron (RMN-Ireland) Foundation and the Irish Motor Neuron Disease Association (IMNDA). The sponsors of this study had no impact on the contents, analyses, and conclusions of this paper or the decision to submit it for publication.

Authors' contributions: FC, EK, IE, and PB contributed to conception and design of the study. FC, MR, VZ, SX, PF, and IP contributed to acquisition and analysis of clinical data. FC, EK, GV, GA, VP, and PB contributed to acquisition and analysis of radiological data. Drafting the manuscript, computational imaging statistics, and generation of figures were carried out by FC, EK, and PB. Revising the manuscript critically for important intellectual content was carried out by NK, IS, IE, and PB. Approval of the manuscript was done by all authors.

References

Abdulla, S., Machts, J., Kaufmann, J., Patrick, K., Kollewe, K., Dengler, R., Heinze, H.J., Petri, S., Vielhaber, S., Nestor, P.J., 2014. Hippocampal degeneration in patients with amyotrophic lateral sclerosis. Neurobiol. Aging 35, 2639–2645.

Abrahams, S., Goldstein, L.H., Lloyd, C.M., Brooks, D.J., Leigh, P.N., 1995a. Cognitive deficits in non-demented amyotrophic lateral sclerosis patients: a neuropsychological investigation. J. Neurol. Sci. 129 (Suppl), 54–55.

Abrahams, S., Leigh, P.N., Kew, J.J., Goldstein, L.H., Lloyd, C.M., Brooks, D.J., 1995b. A positron emission tomography study of frontal lobe function (verbal fluency) in amyotrophic lateral sclerosis. J. Neurol. Sci. 129, 44–46.

Abrahams, S., Newton, J., Niven, E., Foley, J., Bak, T.H., 2014. Screening for cognition and behaviour changes in ALS. Amyotroph. Lateral Scler. Frontotemporal Degener. 15, 9–14.

Allen, D.N., Goldstein, G., 2013. Cluster Analysis in Neuropsychological Research Recent Applications. Springer New York, New York, NY.

Baron, C.A., Beaulieu, C., 2015. Acquisition strategy to reduce cerebrospinal fluid partial volume effects for improved DTI tractography. Magn. Reson. Med. 73, 1075–1084.

Barritt, A.W., Gabel, M.C., Cercignani, M., Leigh, P.N., 2018. Emerging magnetic resonance imaging techniques and analysis methods in amyotrophic lateral sclerosis. Front. Neurol. 9, 1065.

Bede, P., Hardiman, O., 2014. Lessons of ALS imaging: pitfalls and future directions - a critical review. Neuroimage Clin. 4, 436–443.

Bede, P., Hardiman, O., 2018. Longitudinal structural changes in ALS: a three time-point imaging study of white and gray matter degeneration. Amyotroph. Lateral Scler. Frontotemporal Degener. 19, 232–241.

Bede, P., Bokde, A., Elamin, M., Byrne, S., McLaughlin, R.L., Jordan, N., Hampel, H., Gallagher, L., Lynch, C., Fagan, A.J., Pender, N., Hardiman, O., 2013a. Grey matter correlates of clinical variables in amyotrophic lateral sclerosis (ALS): a neuroimaging study of ALS motor phenotype heterogeneity and cortical focality. J. Neurol. Neurosurg. Psychiatry 84, 766–773.

Bede, P., Elamin, M., Byrne, S., McLaughlin, R.L., Kenna, K., Vajda, A., Pender, N., Bradley, D.G., Hardiman, O., 2013b. Basal ganglia involvement in amyotrophic lateral sclerosis. Neurology 81, 2107–2115.

Bede, P., Omer, T., Finegan, E., Chipika, R.H., Iyer, P.M., Doherty, M.A., Vajda, A., Pender, N., McLaughlin, R.L., Hutchinson, S., Hardiman, O., 2018a. Connectivity-based characterisation of subcortical grey matter pathology in frontotemporal dementia and ALS: a multimodal neuroimaging study. Brain Imaging Behav. 12, 1696–1707.

Bede, P., Querin, G., Pradat, P.F., 2018b. The changing landscape of motor neuron disease imaging: the transition from descriptive studies to precision clinical tools. Curr. Opin. Neurol. 31, 431–438.

Beeldman, E., Raaphorst, J., Klein Twennaar, M., de Visser, M., Schmand, B.A., de Haan, R.J., 2016. The cognitive profile of ALS: a systematic review and meta-analysis update. J. Neurol. Neurosurg. Psychiatry 87, 611–619.

Braak, H., Brettschneider, J., Ludolph, A.C., Lee, V.M., Trojanowski, J.Q., Tredici, K.D., 2013. Amyotrophic lateral sclerosis—a model of corticofugal axonal spread. Nat. Rev. Neurol. 9, 708–714.

Brettschneider, J., Del Tredici, K., Toledo, J.B., Robinson, J.L., Irwin, D.J., Grossman, M., Suh, E., Van Deerlin, V.M., Wood, E.M., Baek, Y., Kwong, L., Lee, E.B., Elman, L., McCluskey, L., Fang, L., Feldengut, S., Ludolph, A.C., Lee, V.M., Braak, H.,

Trojanowski, J.Q., 2013. Stages of pTDP-43 pathology in amyotrophic lateral sclerosis. Ann. Neurol. 74, 20–38.
Bueno, A.P.A., Pinaya, W.H.L., Moura, L.M., Bertoux, M., Radakovic, R., Kiernan, M.C., Teixeira, A.L., de Souza, L.C., Hornberger, M., Sato, J.R., 2018. Structural and functional papez circuit integrity in amyotrophic lateral sclerosis. Brain Imaging Behav. 12, 1622–1630.
Burke, T., Lonergan, K., Pinto-Grau, M., Elamin, M., Bede, P., Madden, C., Hardiman, O., Pender, N., 2017a. Visual encoding, consolidation, and retrieval in amyotrophic lateral sclerosis: executive function as a mediator, and predictor of performance. Amyotroph. Lateral Scler. Frontotemporal Degener. 18, 193–201.
Burke, T., Pinto-Grau, M., Lonergan, K., Bede, P., O'Sullivan, M., Heverin, M., Vajda, A., McLaughlin, R.L., Pender, N., Hardiman, O., 2017b. A Cross-sectional population-based investigation into behavioral change in amyotrophic lateral sclerosis: subphenotypes, staging, cognitive predictors, and survival. Ann. Clin. Transl. Neurol. 4, 305–317.
Burke, T., Pinto-Grau, M., Lonergan, K., Elamin, M., Bede, P., Costello, E., Hardiman, O., Pender, N., 2016. Measurement of social cognition in amyotrophic lateral sclerosis: a population based study. PLoS One 11, e0160850.
Caga, J., Hsieh, S., Highton-Williamson, E., Zoing, M.C., Ramsey, E., Devenney, E., Ahmed, R.M., Hogden, A., Kiernan, M.C., 2018. The burden of apathy for caregivers of patients with amyotrophic lateral sclerosis. Amyotroph. Lateral Scler. Frontotemporal Degener. 19, 599–605.
Caga, J., Hsieh, S., Lillo, P., Dudley, K., Mioshi, E., 2019. The impact of cognitive and behavioral symptoms on ALS patients and their caregivers. Front. Neurol. 10, 192.
Cardenas, A.M., Sarlls, J.E., Kwan, J.Y., Bageac, D., Gala, Z.S., Danielian, L.E., Ray-Chaudhury, A., Wang, H.W., Miller, K.L., Foxley, S., Jbabdi, S., Welsh, R.C., Floeter, M.K., 2017. Pathology of callosal damage in ALS: an ex-vivo, 7 T diffusion tensor MRI study. Neuroimage Clin. 15, 200–208.
Chad, J.A., Pasternak, O., Salat, D.H., Chen, J.J., 2018. Re-examining age-related differences in white matter microstructure with free-water corrected diffusion tensor imaging. Neurobiol. Aging 71, 161–170.
Chipika, R.H., Finegan, E., Li Hi Shing, S., Hardiman, O., Bede, P., 2019. Tracking a fast-moving disease: longitudinal markers, monitoring, and clinical trial endpoints in ALS. Front. Neurol. 10, 229.
Christidi, F., Karagiozou, E., Triantafyllou, N.I., Paraskevas, G.P., Zalonis, I., 2012. Trail Making Test error analysis in classic motor neuron disease. Neurol. Sci. 34, 1367–1374.
Christidi, F., Karavasilis, E., Rentzos, M., Kelekis, N., Evdokimidis, I., Bede, P., 2018a. Clinical and radiological markers of extra-motor deficits in amyotrophic lateral sclerosis. Front. Neurol. 9, 1005.
Christidi, F., Karavasilis, E., Velonakis, G., Ferentinos, P., Rentzos, M., Kelekis, N., Evdokimidis, I., Bede, P., 2018b. The clinical and radiological spectrum of hippocampal pathology in amyotrophic lateral sclerosis. Front. Neurol. 9, 523.
de Flores, R., La Joie, R., Chetelat, G., 2015. Structural imaging of hippocampal subfields in healthy aging and Alzheimer's disease. Neuroscience 309, 29–50.
Douet, V., Chang, L., 2014. Fornix as an imaging marker for episodic memory deficits in healthy aging and in various neurological disorders. Front Aging Neurosci. 6, 343.
Duvernoy, H.M., Cattin, F., Risold, P.-Y., 2013. The Human Hippocampus Functional Anatomy, Vascularization and Serial Sections with MRI, fourth ed. Springer, Berlin, Heidelberg.
Elamin, M., Phukan, J., Bede, P., Jordan, N., Byrne, S., Pender, N., Hardiman, O., 2011. Executive dysfunction is a negative prognostic indicator in patients with ALS without dementia. Neurology 76, 1263–1269.
Evans, T.E., Adams, H.H.H., Licher, S., Wolters, F.J., van der Lugt, A., Ikram, M.K., O'Sullivan, M.J., Vernooij, M.W., Ikram, M.A., 2018. Subregional volumes of the hippocampus in relation to cognitive function and risk of dementia. Neuroimage 178, 129–135.
Ferentinos, P., Paparrigopoulos, T., Rentzos, M., Zouvelou, V., Alexakis, T., Evdokimidis, I., 2011. Prevalence of major depression in ALS: comparison of a semi-structured interview and four self-report measures. Amyotroph. Lateral Scler. 12, 297–302.
Feron, M., Couillandre, A., Mseddi, E., Termoz, N., Abidi, M., Bardinet, E., Delgadillo, D., Lenglet, T., Querin, G., Welter, M.L., Le Forestier, N., Salachas, F., Bruneteau, G., Del Mar Amador, M., Debs, R., Lacomblez, L., Meininger, V., Pelegrini-Issac, M., Bede, P., Pradat, P.F., de Marco, G., 2018. Extrapyramidal deficits in ALS: a combined biomechanical and neuroimaging study. J. Neurol. 265, 2125–2136.
Finegan, E., Chipika, R.H., Li Hi Shing, S., Doherty, M.A., Hengeveld, J.C., Vajda, A., Donaghy, C., McLaughlin, R.L., Pender, N., Hardiman, O., Bede, P., 2019a. The clinical and radiological profile of primary lateral sclerosis: a population-based study. J Neurol. https://doi.org/10.1007/s00415-019-09473-z.
Finegan, E., Chipika, R.H., Li Hi Shing, S., Hardiman, O., Bede, P., 2019b. Pathological crying and laughing in motor neuron disease: pathobiology, screening, intervention. Front. Neurol. 10, 260.
Finegan, E., Chipika, R.H., Shing, S.L.H., Hardiman, O., Bede, P., 2019c. Primary lateral sclerosis: a distinct entity or part of the ALS spectrum? Amyotroph. Lateral Scler. Frontotemporal Degener. 20, 133–145.
Fischl, B., 2012. FreeSurfer. Neuroimage 62, 774–781.
Floeter, M.K., Danielian, L.E., Braun, L.E., Wu, T., 2018. Longitudinal diffusion imaging across the C9orf72 clinical spectrum. J. Neurol. Neurosurg. Psychiatry 89, 53–60.
Frecker, M.F., Fraser, F.C., Andermann, E., Pryse-Phillips, W.E., 1990. Association between Alzheimer disease and amyotrophic lateral sclerosis? Can. J. Neurol. Sci. 17, 12–14.
Geser, F., Brandmeir, N.J., Kwong, L.K., Martinez-Lage, M., Elman, L., McCluskey, L., Xie, S.X., Lee, V.M., Trojanowski, J.Q., 2008. Evidence of multisystem disorder in whole-brain map of pathological TDP-43 in amyotrophic lateral sclerosis. Arch. Neurol. 65, 636–641.
Good, C.D., Johnsrude, I.S., Ashburner, J., Henson, R.N., Friston, K.J., Frackowiak, R.S., 2001. A voxel-based morphometric study of ageing in 465 normal adult human brains. Neuroimage 14 (1 Pt 1), 21–36.
Haigler, H.J., Cahill, L., Crager, M., Charles, E., 1986. Acetylcholine, aging and anatomy: differential effects in the hippocampus. Brain Res. 362, 157–160.
Hammer, E.M., Hacker, S., Hautzinger, M., Meyer, T.D., Kubler, A., 2008. Validity of the ALS-Depression-Inventory (ADI-12)–a new screening instrument for depressive disorders in patients with amyotrophic lateral sclerosis. J. Affect. Disord. 109, 213–219.
Iglesias, J.E., Augustinack, J.C., Nguyen, K., Player, C.M., Player, A., Wright, M., Roy, N., Frosch, M.P., McKee, A.C., Wald, L.L., Fischl, B., Van Leemput, K., 2015. A computational atlas of the hippocampal formation using ex vivo, ultra-high resolution MRI: application to adaptive segmentation of in vivo MRI. Neuroimage 115, 117–137.
Ishaque, A., Mah, D., Seres, P., Luk, C., Eurich, D., Johnston, W., Yang, Y.H., Kalra, S., 2018. Evaluating the cerebral correlates of survival in amyotrophic lateral sclerosis. Ann. Clin. Transl. Neurol. 5, 1350–1361.
Jenkinson, M., Smith, S., 2001. A global optimisation method for robust affine registration of brain images. Med. Image Anal. 5, 143–156.
Lomen-Hoerth, C., Murphy, J., Langmore, S., Kramer, J.H., Olney, R.K., Miller, B., 2003. Are amyotrophic lateral sclerosis patients cognitively normal? Neurology 60, 1094–1097.
Ludolph, A., Drory, V., Hardiman, O., Nakano, I., Ravits, J., Robberecht, W., Shefner, J., WFN Research Group On ALS/MND, 2015. A revision of the El Escorial criteria - 2015. Amyotroph. Lateral Scler. Frontotemporal Degener. 16, 291–292.
Machts, J., Bittner, V., Kasper, E., Schuster, C., Prudlo, J., Abdulla, S., Kollewe, K., Petri, S., Dengler, R., Heinze, H.J., Vielhaber, S., Schoenfeld, M.A., Bittner, D.M., 2014. Memory deficits in amyotrophic lateral sclerosis are not exclusively caused by executive dysfunction: a comparative neuropsychological study of amnestic mild cognitive impairment. BMC Neurosci. 15, 83.
Machts, J., Loewe, K., Kaufmann, J., Jakubiczka, S., Abdulla, S., Petri, S., Dengler, R., Heinze, H.J., Vielhaber, S., Schoenfeld, M.A., Bede, P., 2015. Basal ganglia pathology in ALS is associated with neuropsychological deficits. Neurology 85, 1301–1309.
Machts, J., Vielhaber, S., Kollewe, K., Petri, S., Kaufmann, J., Schoenfeld, M.A., 2018. Global hippocampal volume reductions and local CA1 shape deformations in amyotrophic lateral sclerosis. Front. Neurol. 9, 565.
McKhann, G.M., Knopman, D.S., Chertkow, H., Hyman, B.T., Jack Jr., C.R., Kawas, C.H., Klunk, W.E., Koroshetz, W.J., Manly, J.J., Mayeux, R., Mohs, R.C., Morris, J.C., Rossor, M.N., Scheltens, P., Carrillo, M.C., Thies, B., Weintraub, S., Phelps, C.H., 2011. The diagnosis of dementia due to Alzheimer's disease: recommendations from the National Institute on Aging-Alzheimer's Association workgroups on diagnostic guidelines for Alzheimer's disease. Alzheimers Dement. 7, 263–269.
Messinis, L., Tsakona, I., Malefaki, S., Papathanasopoulos, P., 2007. Normative data and discriminant validity of Rey's Verbal Learning Test for the Greek adult population. Arch. Clin. Neuropsychol. 22, 739–752.
Metzler-Baddeley, C., O'Sullivan, M.J., Bells, S., Pasternak, O., Jones, D.K., 2012. How and how not to correct for CSF-contamination in diffusion MRI. Neuroimage 59, 1394–1403.
Meyers, J.E., Meyers, K.R., 1995. Rey Complex Figure Test and Recognition Trial: Professional Manual. Psychological Assessment Resources, Odessa.
Mitsumoto, H., Brooks, B.R., Silani, V., 2014. Clinical trials in amyotrophic lateral sclerosis: why so many negative trials and how can trials be improved? Lancet Neurol. 13, 1127–1138.
Mok, K.Y., Koutsis, G., Schottlaender, L.V., Polke, J., Panas, M., Houlden, H., 2012. High frequency of the expanded C9ORF72 hexanucleotide repeat in familial and sporadic Greek ALS patients. Neurobiol. Aging 33, 1851.e1–1851.e5.
Montuschi, A., Iazzolino, B., Calvo, A., Moglia, C., Lopiano, L., Restagno, G., Brunetti, M., Ossola, I., Lo Presti, A., Cammarosano, S., Canosa, A., Chio, A., 2015. Cognitive correlates in amyotrophic lateral sclerosis: a population-based study in Italy. J. Neurol. Neurosurg. Psychiatry 86, 168–173.
Nasseroleslami, B., Dukic, S., Broderick, M., Mohr, K., Schuster, C., Gavin, B., McLaughlin, R., Heverin, M., Vajda, A., Iyer, P.M., Pender, N., Bede, P., Lalor, E.C., Hardiman, O., 2017. Characteristic increases in EEG connectivity correlate with changes of structural MRI in amyotrophic lateral sclerosis. Cereb. Cortex. 29, 27–41.
Nowrangi, M.A., Rosenberg, P.B., 2015. The fornix in mild cognitive impairment and Alzheimerâ€™s disease. Front. Aging Neurosci. 7, 1.
Olney, R.K., Murphy, J., Forshew, D., Garwood, E., Miller, B.L., Langmore, S., Kohn, M.A., Lomen-Hoerth, C., 2005. The effects of executive and behavioral dysfunction on the course of ALS. Neurology 65, 1774–1777.
Omer, T., Finegan, E., Hutchinson, S., Doherty, M., Vajda, A., McLaughlin, R.L., Pender, N., Hardiman, O., Bede, P., 2017. Neuroimaging patterns along the ALS-FTD spectrum: a multiparametric imaging study. Amyotroph. Lateral Scler. Frontotemporal Degener. 18, 611–623.
Phukan, J., Elamin, M., Bede, P., Jordan, N., Gallagher, L., Byrne, S., Lynch, C., Pender, N., Hardiman, O., 2012. The syndrome of cognitive impairment in

amyotrophic lateral sclerosis: a population-based study. J. Neurol. Neurosurg. Psychiatry 83, 102–108.
Pinto-Grau, M., Hardiman, O., Pender, N., 2018. The study of language in the amyotrophic lateral sclerosis - frontotemporal spectrum disorder: a systematic review of findings and new perspectives. Neuropsychol. Rev. 28, 251–268.
Pyra, T., Hui, B., Hanstock, C., Concha, L., Wong, J.C., Beaulieu, C., Johnston, W., Kalra, S., 2010. Combined structural and neurochemical evaluation of the corticospinal tract in amyotrophic lateral sclerosis. Amyotroph. Lateral Scler. 11, 157–165.
Querin, G., Bede, P., Marchand-Pauvert, V., Pradat, P.F., 2018. Biomarkers of spinal and bulbar muscle atrophy (SBMA): a comprehensive review. Front. Neurol. 9, 844.
Querin, G., El Mendili, M.M., Lenglet, T., Behin, A., Stojkovic, T., Salachas, F., Devos, D., Le Forestier, N., Del Mar Amador, M., Debs, R., Lacomblez, L., Meninger, V., Bruneteau, G., Cohen-Adad, J., Lehericy, S., Laforet, P., Blancho, S., Benali, H., Catala, M., Li, M., Marchand-Pauvert, V., Hogrel, J.Y., Bede, P., Pradat, P.F., 2019. The spinal and cerebral profile of adult spinal-muscular atrophy: a multimodal imaging study. Neuroimage Clin. 21, 101618.
Rabin, J.S., Perea, R.D., Buckley, R.F., Johnson, K.A., Sperling, R.A., Hedden, T., 2019. Synergism between fornix microstructure and beta-amyloid accelerates memory decline in clinically normal older adults. Neurobiol. Aging 81, 38–46.
Schmidt, R., de Reus, M.A., Scholtens, L.H., van den Berg, L.H., van den Heuvel, M.P., 2016. Simulating disease propagation across white matter connectome reveals anatomical substrate for neuropathology staging in amyotrophic lateral sclerosis. Neuroimage 124, 762–769.
Schuster, C., Elamin, M., Hardiman, O., Bede, P., 2015. Presymptomatic and longitudinal neuroimaging in neurodegeneration–from snapshots to motion picture: a systematic review. J. Neurol. Neurosurg. Psychiatry 86, 1089–1096.
Schuster, C., Hardiman, O., Bede, P., 2016. Development of an automated MRI-based diagnostic protocol for amyotrophic lateral sclerosis using disease-specific pathognomonic features: a quantitative disease-state classification study. PLoS One 11, e0167331.
Schuster, C., Hardiman, O., Bede, P., 2017. Survival prediction in Amyotrophic lateral sclerosis based on MRI measures and clinical characteristics. BMC Neurol. 17, 73.
Segers, K., Kadhim, H., Colson, C., Duttmann, R., Glibert, G., 2012. Adult polyglucosan body disease masquerading as "ALS with dementia of the Alzheimer type": an exceptional phenotype in a rare pathology. Alzheimer Dis. Assoc. Disord. 26, 96–99.
Smith, S.M., Jenkinson, M., Woolrich, M.W., Beckmann, C.F., Behrens, T.E., Johansen-Berg, H., Bannister, P.R., De Luca, M., Drobnjak, I., Flitney, D.E., Niazy, R.K., Saunders, J., Vickers, J., Zhang, Y., De Stefano, N., Brady, J.M., Matthews, P.M., 2004. Advances in functional and structural MR image analysis and implementation as FSL. Neuroimage 23 (Suppl 1), S208–S219.
Smith, S.M., Nichols, T.E., 2009. Threshold-free cluster enhancement: addressing problems of smoothing, threshold dependence and localisation in cluster inference. Neuroimage 44, 83–98.
Song, S.K., Yoshino, J., Le, T.Q., Lin, S.J., Sun, S.W., Cross, A.H., Armstrong, R.C., 2005. Demyelination increases radial diffusivity in corpus callosum of mouse brain. Neuroimage 26, 132–140.
Sun, S.W., Liang, H.F., Trinkaus, K., Cross, A.H., Armstrong, R.C., Song, S.K., 2006. Noninvasive detection of cuprizone induced axonal damage and demyelination in the mouse corpus callosum. Magn. Reson. Med. 55, 302–308.
Takeda, T., Uchihara, T., Arai, N., Mizutani, T., Iwata, M., 2009. Progression of hippocampal degeneration in amyotrophic lateral sclerosis with or without memory impairment: distinction from Alzheimer disease. Acta Neuropathol. 117, 35–44.
Westeneng, H.J., Verstraete, E., Walhout, R., Schmidt, R., Hendrikse, J., Veldink, J.H., van den Heuvel, M.P., van den Berg, L.H., 2015. Subcortical structures in amyotrophic lateral sclerosis. Neurobiol. Aging 36, 1075–1082.
Yesavage, J.A., Brink, T.L., Rose, T.L., Lum, O., Huang, V., Adey, M., Leirer, V.O., 1982. Development and validation of a geriatric depression screening scale: a preliminary report. J. Psychiatr. Res. 17, 37–49.
Zalonis I, C.F., Kolovou, D., Pantes, G., Sgouropoulos, P., Vassilopoulos, D., 2008. Assessing Episodic Memory: Normative Data and Discriminant Properties for a Greek Version of Babcock Story Recall Test. In: 3rd Dual Congress on Psychiatry and Neurosciences, Athens.
Zhang, Y., Brady, M., Smith, S., 2001. Segmentation of brain MR images through a hidden Markov random field model and the expectation-maximization algorithm. IEEE Trans. Med. Imaging 20, 45–57.
Zheng, F., Cui, D., Zhang, L., Zhang, S., Zhao, Y., Liu, X., Liu, C., Li, Z., Zhang, D., Shi, L., Liu, Z., Hou, K., Lu, W., Yin, T., Qiu, J., 2018. The volume of hippocampal subfields in relation to decline of memory Recall across the adult lifespan. Front. Aging Neurosci. 10, 320.